International Journal of Heat and Fluid Flow 30 (2009) 20–31

Contents lists available at ScienceDirect

International Journal of Heat and Fluid Flow

journal homepage: www.elsevier.com/locate/ijhff

Log-layer mismatch and commutation error in hybrid RANS/LES simulation of channel flow

Fujihiro Hamba

Institute of Industrial Science, University of Tokyo, 4-6-1 Komaba, Meguro-ku, Tokyo 153-8505, Japan

ARTICLE INFO

Article history:
Received 14 March 2008
Received in revised form 15 August 2008
Accepted 18 October 2008
Available online 30 November 2008

Keywords:
RANS
LES
Hybrid
Channel flow

ABSTRACT

Hybrid approach combining large eddy simulation (LES) with the Reynolds-averaged Navier–Stokes equation (RANS) is expected to accurately simulate wall-bounded turbulent flows at high Reynolds numbers. As an important issue in developing hybrid methods, it is known that the log layers in the RANS and LES regions are not lined up in hybrid RANS/LES simulations of channel flow. Although several methods including additional filtering near the RANS/LES interface have been proposed to eliminate the log-layer mismatch, there is no obvious physical justification for the methods and some ad hoc tuning is necessary. In this work, the commutation error terms in the filtered velocity equations are investigated to justify the method of additional filtering. It is shown that the additional filtering can be considered as a finite difference approximation to extra terms due to the non-commutivity between the hybrid filter and the spatial derivative. Moreover, an expression determining the filter width and its location for the additional filtering is obtained. To validate the expression, a hybrid simulation of channel flow is carried out. The additional filtering with the filter width derived is shown to be effective in eliminating the log-layer mismatch and improving the mean velocity profile.

1. Introduction

Reynolds-averaged Navier–Stokes equation (RANS) models have been widely used for simulations of turbulent flows at high Reynolds numbers (Hanjalic, 2005). Various RANS models have been proposed and improved; they accurately predict simple equilibrium flows. However, unsteady behavior of non-equilibrium flows cannot be adequately reproduced by RANS. As an alternative, large eddy simulation (LES) has been developed to successfully predict non-equilibrium flows. The rapid development of computer has enabled the LES of practical engineering flows in relatively complex geometries. Nevertheless, it is still impossible to simulate wall-bounded flows at high Reynolds numbers with the no-slip boundary condition. This limitation is because a large number of grid points are required to resolve small vortex structures near the wall.

To simulate high-Reynolds-number wall-bounded flows more accurately, hybrid approaches have been proposed that combine LES with RANS. A RANS model is solved near the wall with the no-slip boundary condition whereas LES is carried out away from the wall. Detached eddy simulation (DES) proposed by Spalart et al. (1997) is one of hybrid simulations for massively separated flows. In DES, the Spalart–Allmaras RANS model (Spalart and Allmaras, 1994) is extended to an LES model; the simulation is switched from RANS to LES by comparing the distance from the wall with the local grid spacing. In addition to DES, several hybrid simulations were proposed. When the Smagorinsky model is used for LES, it is natural to adopt a zero-equation model for RANS such as Cebeci-Smith and Baldwin-Lomax models for aerodynamics flows (Georgiadis et al., 2003; Kawai and Fujii, 2005). For more general flows, one-equation and two-equation RANS models need to be adopted such as k–l, k–ω, and k–ε models (Davidson and Peng, 2003; Hamba, 2003; Batten et al., 2004; Tucker and Davidson, 2004; Davidson and Dahlström, 2005; Temmerman et al., 2005; Abe, 2005; Schiestel and Dejoan, 2005; Befeno and Schiestel, 2007; Breuer et al., 2008).

Although these hybrid approaches are the same in the sense that RANS and LES are combined, the objective of DES is somewhat different from others. In DES, the RANS model was originally developed to accurately predict the attached boundary layer around a object such as an airplane wing. In order to successfully predict unsteady behavior of the separated region away from the object, the simulation is switched to LES outside the attached boundary layer. Therefore, the whole attached boundary layer should be simulated by RANS and only the separated flow is calculated by LES; the model is switched at the edge of the attached boundary layer. On the other hand, other hybrid simulations were often developed for better wall modeling of LES. Since LES is expected to accurately predict turbulent flows, it is applied to most of the computational region including the attached boundary layer. Only in the near-wall region where the grid spacing is too large to capture the small

E-mail address: hamba@iis.u-tokyo.ac.jp

0142-727X/$ - see front matter © 2008 Elsevier Inc. All rights reserved.
doi:10.1016/j.ijheatfluidflow.2008.10.002

structure, a RANS model is used as an accurate wall model for LES; the model is switched inside the attached boundary layer. Therefore, the location of the RANS/LES interface in DES should be different from that in the wall-modeled LES. However, there seems to be some confusion between DES and the other approaches (Spalart et al., 2006). One of the reason for the confusion is that in the original DES, the model can be switched inside the boundary layer for some fine grid in spite of the objective of DES. In fact, Nikitin et al. (2000) showed results of the LES of channel flow in which DES is used as a wall model and the RANS/LES interface is set inside the boundary layer. Recently, Spalart et al. (2006) proposed the delayed DES to simulate the whole boundary layer by RANS for any type of grid. The delayed DES clarifies the standpoint of DES relative to the wall-modeled LES.

There are several important issues in developing hybrid methods. For example, Nikitin et al. (2000) reported that in the DES-based wall-modeled LES of channel flow, an unphysical buffer layer appears near the RANS/LES interface and the log layers in the RANS and LES regions are not lined up. Owing to the log-layer mismatch the skin-friction coefficient is underpredicted by approximately 15% in most cases. Using a similar method, Radhakrishnan et al. (2006) carried out the wall-modeled LES of non-equilibrium flows such as the flow past a bump and examined the RANS/LES interface dynamics. They found that the skin-friction coefficient is underpredicted in the equilibrium upstream region whereas the performance is improved in the non-equilibrium region after the separation. The log-layer mismatch was also reported in other hybrid simulations. In a hybrid simulation using the k–ω model (Davidson and Peng, 2003), the mean velocity profile shows a kink at the interface. In another hybrid simulation using the k–ε model (Hamba, 2001), similar log-layer mismatch is seen although the positions of the RANS and LES regions are reversed compared to the normal hybrid method. Therefore, the log-layer mismatch is a problem commonly seen in hybrid simulations.

In the natural DES approach, the log-layer mismatch is not apparent because the whole boundary layer is simulated by RANS only. On the other hand, it can be a serious problem for the wall-modeled LES. It is important to understand the reason for the log-layer mismatch and to develop a method for eliminating it. Piomelli et al. (2003) applied a stochastic back-scatter model to the DES-based wall-modeled LES of channel flow. They showed that the model is effective in improving the prediction of the mean velocity profile. Using the mixing-length and k–ε models for RANS, Hamba (2003, 2006) carried out hybrid simulations of channel flow and introduced additional filtering at the interface to reduce the log-layer mismatch. Although these methods were shown to be effective, the amplitude of the stochastic forcing and the width of the additional filtering need to be determined empirically. Recently, Keating and Piomelli (2006) proposed a dynamic method to determine the forcing amplitude by considering the difference between the resolved and modeled shear stresses in the transition region. Although the log-layer mismatch is removed, the magnitude of the stochastic forcing is very large; it is not yet clear whether such a stochastic forcing is justified physically. As other approaches, Davidson and Dahlström (2005) proposed to add turbulent fluctuations, obtained from the direct numerical simulation (DNS), to the momentum equation. Temmerman et al. (2005) found that by feeding the instantaneous value of the eddy-viscosity coefficient at the interface, the anomaly of the mean velocity profile diminished. Larsson et al. (2007) used an additional forcing to investigate the behavior of the artificial buffer layer and proposed a low-dimensional forcing model. In the limited-numerical-scale approach proposed by Batten et al. (2004), synthetic turbulence is generated to automatically convert the statistical turbulent energy in the RANS region into resolved-scale velocity fluctuations in the LES region through interface.

In usual zonal hybrid approach, the location of the RANS/LES interface is clearly defined. In contrast, Breuer et al. (2008) used the local value of modeled turbulent energy as switching condition; the interface location is determined dynamically and fluctuates in space and in time. They compared results obtained from the dynamical interface with that from the sharp interface in channel and hill flows. On the other hand, non-zonal hybrid approach has also been developed which seamlessly bridges RANS and LES. Schiestel and Dejoan (2005) derived a new equation for the energy dissipation rate for LES and applied a non-zonal hybrid k–ϵ model to homogeneous turbulence and channel flow. This non-zonal hybrid model was also applied to shearless mixing layer (Befeno and Schiestel, 2007) and to thermal convection at high Rayleigh numbers (Kenjereš and Hanjalić, 2006).

The problem of the solution discontinuity at the interface is not restricted to the RANS/LES method, but also holds for multi-resolution LES (Quéméré et al., 2001). Both RANS/LES and multi-resolution LES can be seen as particular cases of a general multi-domain/multi-resolution method (Sagaut et al., 2006). Using the interface condition originally developed for multi-resolution LES, Quéméré and Sagaut (2002) carried out RANS/LES simulations of the plane channel and the plane plate with a trailing-edge configurations. On the basis of the multi-resolution LES, other RANS/LES approaches were also developed in which the mean flow is computed using RANS while resolved fluctuations are derived from LES (Labourasse and Sagaut, 2002; Benarafa et al., 2006).

In order to justify and improve hybrid approaches it is necessary to investigate the method of combining RANS with LES from a theoretical point of view. Recently, Germano (2004) defined a hybrid RANS/LES filter and formulated the filtered velocity equations. He showed that several extra terms appear in the filtered Navier–Stokes and continuity equations because of the non-commutivity between the hybrid filter and the spatial derivative. The extra terms can have non-zero values near the RANS/LES interface although they are neglected in hybrid simulations. Therefore, we expect that the investigation of the commutation error gives a clue to improving the hybrid approaches including the stochastic forcing and the additional filtering.

In this work, we examine the extra terms due to the non-commutivity to physically justify the additional filtering at the interface. In the following section, we briefly explain the log-layer mismatch and the additional filtering in channel flow simulation. In Section 3, we introduce a two-dimensional filtering with the filter width ranging from the grid size to the RANS length scale. We examine the filtered continuity and Navier–Stokes equations and investigate the relation between the additional filtering and the extra terms due to the non-commutivity. We also obtain an expression determining the filter width and its location for the additional filtering. In Section 4, we apply the expression to a hybrid simulation of channel flow to assess its validity. Concluding remarks are given in Section 5.

2. Log-layer mismatch and additional filtering

It is known that in hybrid RANS/LES simulations of channel flow, an unphysical buffer layer appears near the RANS/LES interface and the log layers in the RANS and LES regions are not lined up (Davidson and Peng, 2003; Hamba, 2003; Nikitin et al., 2000; Piomelli et al., 2003). A mechanism for the log-layer mismatch can be described as follows (Hamba, 2003, 2006; Piomelli et al., 2003). In the RANS region near the wall, the resolved velocity fluctuations are weak and their length scale is large owing to the large turbulent viscosity. Ideally, intense small-scale fluctuations of the resolved velocity field should be quickly recovered as the wall-normal coordinate increases across the RANS/LES interface; the re-

solved velocity fluctuations should be dominant in the LES region. However, the velocity field in the RANS region can non-locally affect the velocity field at the bottom of the LES region (Hamba, 2005). In fact, the so-called super-streaks, or large regions of strong positive and negative streamwise velocity fluctuations in the RANS region are still observed at $y^+ \simeq 1000$ in the LES region where y^+ is the wall-normal coordinate in wall unit (Piomelli et al., 2003). Consequently, the velocity fluctuations at the bottom of the LES region are reduced artificially and their length scale is too large; the resolved shear stress is underpredicted compared to that in standard LES. On the other hand, the total of the resolved, modeled, and viscous stress terms needs to be equal to the constant pressure-gradient term in the mean velocity equation. This balance requires that the modeled and viscous stress terms should have larger values. Since the modeled and viscous stresses are proportional to the mean velocity gradient, it has to be overpredicted near the interface, leading to an unphysical buffer layer.

Several attempts have been made to eliminate the log-layer mismatch (Hamba, 2003, 2006; Davidson and Dahlström, 2005; Temmerman et al., 2005; Piomelli et al., 2003; Keating and Piomelli, 2006). Stochastic forcing is a candidate for generating intense small-scale fluctuations of the resolved velocity field to diminish the unphysical buffer layer. Piomelli et al. (2003) introduced a stochastic back-scatter model; they added a forcing term f_i to the momentum equation. The forcing is obtained from a series of Gaussian random numbers and its amplitude envelope is given by

$$f(y) = A\frac{(\lambda y)^2}{1+(\lambda y)^4}, \tag{1}$$

where $\lambda = 30$ is chosen for the peak of $f(y)$ to be located near the RANS/LES interface and the amplitude A is determined empirically. As a result, the stochastic forcing can break up the super-streaks and generate smaller scales near the interface; the log-layer mismatch can be eliminated.

On the other hand, Hamba (2003) introduced additional filtering at the RANS/LES interface to remove the log-layer mismatch. In this method, stochastic forcing is not applied but two different velocity components are introduced at the interface. Fig. 1 shows grid cells and velocity components near the RANS/LES interface; only the x–y plane is shown for simplicity. The variables x, y, and z denote the coordinates in the streamwise, wall-normal, and spanwise directions, respectively; corresponding components of the resolved velocity field are given by $\bar{u}$, $\bar{v}$, and $\bar{w}$. In the x–z planes at $y_A^+ < y^+ < y_B^+$, additional filtering denoted by $\hat{\cdot}$ is introduced to define two different velocities $\bar{\mathbf{u}}$ and $\hat{\bar{\mathbf{u}}}$. For example, the discretized forms of the continuity equation for cells (i,j) and $(i,j+1)$ shown in Fig. 1 can be written as

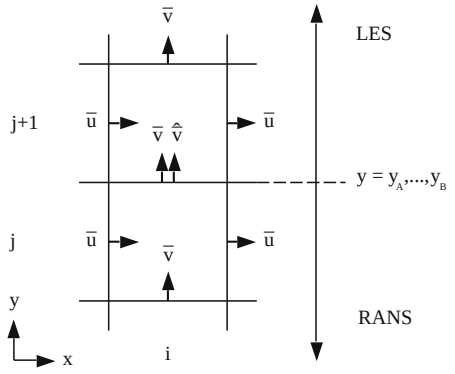

Fig. 1. Grid cells and velocity components near the RANS/LES interface in the method of additional filtering.

$$\left(\frac{\partial\bar{u}}{\partial x}+\frac{\partial\bar{w}}{\partial z}\right)_{ij}+\frac{\hat{\bar{v}}_{ij+1/2}-\bar{v}_{ij-1/2}}{\Delta y}=0, \tag{2}$$

$$\left(\frac{\partial\bar{u}}{\partial x}+\frac{\partial\bar{w}}{\partial z}\right)_{ij+1}+\frac{\bar{v}_{ij+3/2}-\hat{\bar{v}}_{ij+1/2}}{\Delta y}=0, \tag{3}$$

where indices i and j denote the nodes in the x and y directions, respectively, Δy is the grid spacing in the y direction, and discretized forms of the x- and z-derivatives are omitted. These equations mean that the component $\bar{v}_{ij+1/2}$ at the interface is referred to from cell $(i,j+1)$ in the LES region whereas $\hat{\bar{v}}_{ij+1/2}$ is referred to from cell (i,j) in the RANS region. Because of the additional filtering, the fluctuation of $\hat{\bar{v}}_{ij+1/2}$ is weak and its length scale is large compared to those of $\bar{v}_{ij+1/2}$. It is expected that the underprediction of the intensity of $\bar{v}_{ij+1/2}$ can be corrected by distinguishing the two components. The same filtering is also applied to the convection terms in the Navier–Stokes equation such as $\widehat{\bar{u}\bar{v}}$ at point $(i+1/2,j+1/2)$. As a result, the log-layer mismatch can be reduced and good velocity profiles are obtained (Hamba, 2003, 2006).

Let us mention the conservation properties of the government equations. In Eqs. (2) and (3), different components $\hat{\bar{v}}_{ij+1/2}$ and $\bar{v}_{ij+1/2}$ are defined at point $(i,j+1/2)$; mass is not conserved locally. This is because the filter width, or the length scale for local volume average, is different between cells (i,j) and $(i,j+1)$. However, since the relation $\langle\hat{\bar{v}}_{ij+1/2}\rangle = \langle\bar{v}_{ij+1/2}\rangle$ holds where $\langle\cdot\rangle$ denotes the x–z plane average, mass is conserved globally. The same holds for the convection terms; the global conservation of momentum is satisfied as $\langle\widehat{\bar{u}\bar{v}}_{i+1/2,j+1/2}\rangle = \langle\bar{u}\bar{v}_{i+1/2,j+1/2}\rangle$.

It was shown that the two methods described here are effective in eliminating the log-layer mismatch. However, there is no obvious physical justification for the methods and ad hoc tuning of the forcing amplitude or the filter width is required. Recently, Keating and Piomelli (2006) proposed a dynamic method to determine the forcing amplitude for the back-scatter model. They considered the difference between the resolved and modeled shear stresses in the transition region and determined the amplitude using a control parameter. Although the log-layer mismatch is removed, the magnitude of the stochastic forcing is fairly large; its root-mean-square (RMS) value is up to 80% of the RMS of $d\bar{u}_i/dt$ near the interface. It is not yet clear whether such a strong forcing is justified physically. Further investigation is needed for the methods of the stochastic forcing and the additional filtering.

3. Commutation error in filtered equations

In this section, in order to justify the additional filtering and to derive an expression determining the filter width $\widehat{\Delta}$ for it, we examine the commutation error in the filtered Navier–Stokes and continuity equations.

Germano (2004) proposed a hybrid RANS/LES filter defined as

$$\bar{u}_k = (1-\alpha_G)\bar{u}_k^{\mathrm{LES}} + \alpha_G\langle u_k\rangle, \tag{4}$$

where $\bar{\cdot}^{\mathrm{LES}}$ denotes the LES filter and $\langle\cdot\rangle$ denotes the Reynolds average. The hybrid filter represents LES for $\alpha_G = 0$ and RANS for $\alpha_G = 1$. The blending parameter α_G ($0 \leqslant \alpha_G \leqslant 1$) is a function of the local position and can be chosen arbitrarily. Applying the hybrid filter he derived the filtered Navier–Stokes and continuity equations. For example, the velocity gradient in the equations is written as

$$\overline{\frac{\partial u_k}{\partial x_m}} = \frac{\partial\bar{u}_k}{\partial x_m} + \frac{\partial\alpha_G}{\partial x_m}(\bar{u}_k^{\mathrm{LES}} - \langle u_k\rangle). \tag{5}$$

The second term on the right-hand side is an extra term due to the non-commutivity between the hybrid filter and the spatial derivative. Several extra terms appear in the filtered Navier–Stokes and continuity equations; the neglect of the extra terms in previous hybrid simulations may be responsible for inaccurate velocity profiles.

Although this theoretical formulation must be important, its application is not easy; the evaluation of the LES velocity $\bar{u}_k^{\mathrm{LES}}$ from the hybrid filtered velocity $\bar{u}_k$ must be ill-posed for $\alpha_G \simeq 1$ because $\bar{u}_k \simeq \langle u_k \rangle$ as mentioned in Germano (2004).

Similar extra terms due to the non-commutivity between the filtering and the spatial derivative also appear in the equations for conventional LES (Fureby and Tabor, 1997; Fureby et al., 1997). It is interesting to consider the hybrid simulation as an LES with the filter width ranging from the grid size to the RANS length scale. In general, the gradient of the filter width for conventional LES is not very steep and the commutation error can usually be neglected. On the other hand, the extra terms cannot be neglected in the hybrid simulation because the filter width changes rapidly across the RANS/LES interface. Here, in order to investigate the effect of the extra terms, we assume that the hybrid filter in a channel flow can be given by the following two-dimensional filtering:

$$\bar{u}_k(\mathbf{x}) = \int\int dx'dz' G(x-x', z-z', \alpha) u_k(\mathbf{x}'), \tag{6}$$

where the filter function G is given by

$$G(x,z,\alpha) = \frac{6}{\pi \ell_x \ell_z} \exp\left(-6\left(\frac{x^2}{\ell_x^2} + \frac{z^2}{\ell_z^2}\right)\right), \tag{7}$$

$$\ell_x = \frac{\ell \Delta x}{\sqrt{\Delta x^2 + \Delta z^2}}, \quad \ell_z = \frac{\ell \Delta z}{\sqrt{\Delta x^2 + \Delta z^2}}, \tag{8}$$

$$\ell = \alpha \ell_R. \tag{9}$$

Here α is the blending parameter and ℓ_R is the RANS length scale as long as the integral scale. The parameter α varies from $\alpha_L (= \sqrt{\Delta x^2 + \Delta z^2}/\ell_R)$ to unity; the hybrid filter represents LES for $\alpha = \alpha_L$ and RANS for $\alpha = 1$. The velocity gradient in the filtered equations can then be written as

$$\overline{\frac{\partial u_k}{\partial x_m}} = \frac{\partial \bar{u}_k}{\partial x_m} - \frac{\partial \alpha}{\partial x_m} \int\int dx'dz' \frac{\partial G}{\partial \alpha} u_k(\mathbf{x}') = \frac{\partial \bar{u}_k}{\partial x_m} - \frac{\partial \alpha}{\partial x_m} \frac{\partial \bar{u}_k}{\partial \alpha}. \tag{10}$$

Strictly speaking, the RANS corresponds to $\ell (= \alpha \ell_R) \to \infty$ in this case because the x–z plane average can be considered as the Reynolds average for a channel flow. Here, we assume that ℓ_R is so large that the filtering with $\alpha = 1$ can be approximated as the Reynolds average. We believe that this approximation is not too bad because the second term on the right-hand side of Eq. (10) can be shown to correspond to the extra term in Germano's hybrid filter in Eq. (5) as follows:

$$\frac{\partial \bar{u}_k}{\partial \alpha} = \frac{\bar{u}_k|_{\alpha=1} - \bar{u}_k|_{\alpha=\alpha_L}}{1-\alpha_L} \simeq \langle u_k \rangle - \bar{u}_k^{\mathrm{LES}}, \tag{11}$$

where $\alpha_L \ll 1$ is assumed. Of course, it is not clear whether an LES with the RANS length-scale filtering actually represents the RANS. The definition of a spatial average equivalent to the Reynolds average in general flows is a difficult issue and remains as future work. We should note that we do not explicitly apply the filtering given by Eq. (6) to actual simulations; we introduced this filtering in order to examine the relation between the additional filtering and the extra term due to the non-commutivity.

The filtered continuity and Navier–Stokes equations are written as

$$\overline{\frac{\partial u_k}{\partial x_k}} = \frac{\partial \bar{u}_k}{\partial x_k} - \frac{\partial \alpha}{\partial x_k}\frac{\partial \bar{u}_k}{\partial \alpha} = 0, \tag{12}$$

and

$$\begin{aligned}\frac{\partial \bar{u}_k}{\partial t} &= -\overline{\frac{\partial u_k u_m}{\partial x_m}} - \overline{\frac{\partial p}{\partial x_k}} + \nu \overline{\frac{\partial^2 u_k}{\partial x_m \partial x_m}} \\ &= -\frac{\partial}{\partial x_m}\overline{u_k u_m} + \frac{\partial \alpha}{\partial x_m}\frac{\partial \overline{u_k u_m}}{\partial \alpha} - \frac{\partial \bar{p}}{\partial x_k} + \frac{\partial \alpha}{\partial x_k}\frac{\partial \bar{p}}{\partial \alpha} + \nu \frac{\partial^2 \bar{u}_k}{\partial x_m \partial x_m} + R_k,\end{aligned} \tag{13}$$

respectively, where p is the pressure, ν is the kinetic viscosity, and R_k denotes extra terms associated with the viscous diffusion term. We should note that Eqs. (12) and (13) are exact equations for the filtered velocity when the filter function depends on a parameter α in general (Fureby and Tabor, 1997). Here, we examine the continuity equation (12). For simplicity, we assume that the blending parameter α depends only on the y coordinate and $\partial\alpha/\partial y < 0$. This profile of α corresponds to the lower half of a channel flow. The terms related to the y derivative in Eq. (12) are then written as

$$\overline{\frac{\partial v}{\partial y}} = \frac{\partial \bar{v}}{\partial y} - \frac{\partial \alpha}{\partial y}\frac{\partial \bar{v}}{\partial \alpha}. \tag{14}$$

A second-order finite-difference form of the right-hand side can be written as

$$\begin{aligned}\left(\frac{\partial \bar{v}}{\partial y} - \frac{\partial \alpha}{\partial y}\frac{\partial \bar{v}}{\partial \alpha}\right)_{ij} &= \frac{\bar{v}_{i,j+1/2} - \bar{v}_{i,j-1/2}}{\Delta y} - \frac{\alpha_{j+1/2} - \alpha_{j-1/2}}{\Delta y} \\ &\quad \times \frac{[G(\alpha_{j+1/2}) * v]_{ij} - [G(\alpha_{j-1/2}) * v]_{ij}}{\alpha_{j+1/2} - \alpha_{j-1/2}},\end{aligned} \tag{15}$$

where

$$G(\alpha_{j+1/2}) * f = dx'dz' G(x-x', z-z', \alpha_{j+1/2}) f(\mathbf{x}'). \tag{16}$$

In Eq. (15), a central difference scheme is used for $\partial G/\partial\alpha$, which is evaluated at point (i,j). By applying the following approximations:

$$[G(\alpha_{j+1/2}) * v]_{ij} = \{[G(\alpha_{j+1/2}) * v]_{ij+1/2} + [G(\alpha_{j+1/2}) * v]_{ij-1/2}\}/2, \tag{17}$$

$$\frac{1}{2}[G(\alpha_{j+1/2}) + G(\alpha_{j-1/2})] * v = G(\alpha_j) * v, \tag{18}$$

we obtain a more compact form given by

$$\left(\frac{\partial \bar{v}}{\partial y} - \frac{\partial \alpha}{\partial y}\frac{\partial \bar{v}}{\partial \alpha}\right)_{ij} = \frac{\bar{v}^+_{i,j+1/2} - \bar{v}^-_{ij-1/2}}{\Delta y}, \tag{19}$$

where

$$\bar{v}^+_{i,j+1/2} = [G(\alpha_j) * v]_{i,j+1/2}, \tag{20}$$

$$\bar{v}^-_{ij-1/2} = [G(\alpha_j) * v]_{ij-1/2}. \tag{21}$$

In the definition of $\bar{v}^+_{i,j+1/2}$, the location of the blending parameter α_j is different from that of $\alpha_{j+1/2}$ used for the original component $\bar{v}_{i,j+1/2}$. The same holds for α_j in the definition of $\bar{v}^-_{ij-1/2}$. Since $\alpha_j > \alpha_{j+1/2}$, the velocity $\bar{v}^+_{i,j+1/2}$ is closer to the RANS velocity $\langle v \rangle_{i,j+1/2}$ than $\bar{v}_{i,j+1/2}$ is; that is, the fluctuation level of $\bar{v}^+_{i,j+1/2}$ is lower than that of $\bar{v}_{i,j+1/2}$. In contrast, since $\alpha_j < \alpha_{j-1/2}$, the velocity $\bar{v}^-_{ij-1/2}$ is closer to the LES velocity $\bar{v}^{\mathrm{LES}}_{ij-1/2}$ than $\bar{v}_{ij-1/2}$ is; that is, the fluctuation level of $\bar{v}^-_{ij-1/2}$ is higher than that of $\bar{v}_{ij-1/2}$. We can consider $\bar{v}^+_{i,j+1/2}$ as a kind of filtered value of $\bar{v}_{i,j+1/2}$ and $\bar{v}^-_{ij-1/2}$ as a kind of defiltered value of $\bar{v}_{ij-1/2}$. In our preliminary simulation of channel flow, we used finite difference forms of the filtered and defiltered terms in Eq. (19). However, a statistically steady solution was not obtained because the defiltering scheme was numerically unstable. The defiltering problem must be badly conditioned near the RANS/LES interface because $\alpha_j - \alpha_{j-1/2}$ is not small.

In order to avoid the defiltering, we propose another form of approximation to Eq. (14)

$$\begin{aligned}\left(\frac{\partial \bar{v}}{\partial y} - \frac{\partial \alpha}{\partial y}\frac{\partial \bar{v}}{\partial \alpha}\right)_{ij} &= \frac{\bar{v}_{i,j+1/2} - \bar{v}_{i,j-1/2}}{\Delta y} - \frac{\alpha_{j+1/2} - \alpha_{j-1/2}}{\Delta y} \\ &\quad \times \frac{[G(\alpha_{j+1/2}) * v]_{i,j+1/2} - [G(\alpha_{j-1/2}) * v]_{i,j+1/2}}{\alpha_{j+1/2} - \alpha_{j-1/2}} \\ &= \frac{\bar{v}^{++}_{i,j+1/2} - \bar{v}_{ij-1/2}}{\Delta y},\end{aligned} \tag{22}$$

where

$$\bar{v}^{++}_{i,j+1/2} = [G(\alpha_{j-1/2}) * v]_{i,j+1/2}. \tag{23}$$

In Eq. (22), the term $\partial G/\partial\alpha$ is evaluated at point $(i,j+1/2)$ where $\alpha_{ij+1/2} < \alpha_{ij}$; it is a kind of forward difference scheme of $\partial G/\partial\alpha$. As a result, the filtered value $\bar{v}^{++}_{ij+1/2}$ is used at point $(i,j+1/2)$ whereas the defiltered value is not necessary at point $(i,j-1/2)$. We can see that Eq. (22) takes the same form as the second term on the left-hand side of Eq. (2) discussed in the preceding section; the velocity $\bar{v}^{++}_{ij+1/2}$ in Eq. (22) corresponds to $\hat{\bar{v}}_{ij+1/2}$ in Eq. (2).

In actual simulations the continuity equation is used to derive the Poisson equation for the pressure and the latter equation is solved. The filtered Navier–Stokes equation given by Eq. (13) can be rewritten as

$$\frac{\partial \bar{u}_k}{\partial t} = -\frac{\partial \bar{p}}{\partial x_k} + \overline{F}_k, \tag{24}$$

where $\overline{F}_k$ is the remaining part that does not involve the pressure. Here, the term containing $\partial\bar{p}/\partial\alpha$ is neglected as will be explained in the next section. Taking the divergence of Eq. (24) with Eq. (22) we have

$$\left(\frac{\partial^2\bar{p}}{\partial x^2}+\frac{\partial^2\bar{p}}{\partial z^2}\right)_{ij} + \frac{1}{\Delta y}\left[\left(\frac{\partial \bar{p}^{++}}{\partial y}\right)_{ij+1/2} - \left(\frac{\partial\bar{p}}{\partial y}\right)_{ij-1/2}\right] = \left(\frac{\partial\overline{F}_x}{\partial x}+\frac{\partial\overline{F}_z}{\partial z}\right)_{ij} + \frac{1}{\Delta y}\left[(\overline{F}^{++}_y)_{ij+1/2} - (\overline{F}_y)_{ij-1/2}\right]. \tag{25}$$

This modified Poisson equation for the pressure is solved so that the continuity Eq. (12) can be satisfied.

The additional filtering applied to the convection term in the Navier–Stokes equation can be written in a similar form to Eq. (22). For example, in Eq. (13) for $\bar{u}_{i+1/2,j}$, one of the convection term can be given by

$$\left(\frac{\partial\overline{u}\overline{v}}{\partial y} - \frac{\partial\alpha}{\partial y}\frac{\partial\overline{u}\overline{v}}{\partial\alpha}\right)_{i+1/2,j} = \frac{\overline{u}\overline{v}^{++}_{i+1/2,j+1/2} - \overline{u}\overline{v}_{i+1/2,j-1/2}}{\Delta y}, \tag{26}$$

where

$$\overline{u}\overline{v}^{++}_{i+1/2,j+1/2} = [G(\alpha_{j-1/2}) * uv]_{i+1/2,j+1/2}. \tag{27}$$

Eq. (26) is also the same form as the convection term used in Hamba (2003).

Moreover, using the property of the Gaussian function we can rewrite Eq. (23) as

$$\bar{v}^{++}_{ij+1/2} = \left[G\left(\sqrt{\alpha^2_{j-1/2}-\alpha^2_{j+1/2}}\right) * G(\alpha_{j+1/2}) * v\right]_{ij+1/2} = \left[G\left(\sqrt{\alpha^2_{j-1/2}-\alpha^2_{j+1/2}}\right) * \bar{v}\right]_{ij+1/2}. \tag{28}$$

This expression gives the relation between $\bar{v}^{++}_{ij+1/2}$ and $\bar{v}_{ij+1/2}$; the former can be obtained from the latter by applying two-dimensional filtering with the filter width

$$\widehat{\Delta}_{j+1/2} = \sqrt{\alpha^2_{j-1/2}-\alpha^2_{j+1/2}}\,\ell_{Rj+1/2}. \tag{29}$$

This is indeed the expression determining the filter width and its location for the additional filtering. Therefore, the additional filtering proposed by Hamba (2003) can be considered as a finite difference approximation to the commutation error terms and a specific expression for the filter width $\widehat{\Delta}$ is obtained.

Here, let us mention a possible relation between the defiltered term described above and stochastic forcing proposed by other hybrid simulations (Davidson and Dahlström, 2005; Piomelli et al., 2003). Paying attention to the defiltered term, we can derive another form of the convection term in the Navier–Stokes equation as

$$\left(\frac{\partial\overline{u}\overline{v}}{\partial y} - \frac{\partial\alpha}{\partial y}\frac{\partial\overline{u}\overline{v}}{\partial\alpha}\right)_{i+1/2,j} = \frac{\overline{u}\overline{v}_{i+1/2,j+1/2} - \overline{u}\overline{v}_{i+1/2,j-1/2}}{\Delta y} + \frac{\overline{u}\overline{v}_{i+1/2,j-1/2} - \overline{u}\overline{v}^{--}_{i+1/2,j-1/2}}{\Delta y}, \tag{30}$$

where

$$\overline{u}\overline{v}^{--}_{i+1/2,j-1/2} = [G(\alpha_{j+1/2}) * uv]_{i+1/2,j-1/2}. \tag{31}$$

The second term on the right-hand side of Eq. (30) is an extra term involving the defiltered term. The defiltering in general enhances the velocity fluctuations with short length scales. The stochastic forcing with no spatial correlation also increases small-scale fluctuations. In this sense, the stochastic forcing plays a similar role to the defiltering term in Eq. (30). It is interesting to note that the second term on the right-hand side of Eq. (30) vanishes when the Reynolds average is taken because $\langle\overline{u}\overline{v}^{--}_{i+1/2,j-1/2}\rangle = \langle\overline{u}\overline{v}\rangle_{i+1/2,j-1/2}$. The forcing in the back-scatter model of Piomelli et al. (2003) has zero mean value whereas the net forcing of Davidson and Dahlström (2005) is positive in the streamwise direction. The vanishing of the mean value of the extra term in Eq. (30) suggests that a forcing with zero mean value like Piomelli et al. (2003) is more appropriate.

In the multi-resolution LES, Quéméré et al. (2001) proposed a method for connecting two domains having different resolutions. The restriction and enrichment procedures for variables at the interface correspond to filtering and defiltering, respectively. It must be interesting to apply the additional filtering in the present work to the restriction procedure at the interface as $\hat{\bar{u}}^{\mathrm{LES}}_k = \bar{u}^{\mathrm{RANS}}_k$, which is easier to interpret. On the other hand, in their RANS/LES simulation (Benarafa et al., 2006) added the following body force to the momentum equations:

$$f^{\mathrm{RANS/LES}}_i = W_i\frac{u^{\mathrm{RANS}}_i - \tilde{u}^{\mathrm{LES}}_i}{\alpha_B\Delta t}, \tag{32}$$

where W_i is a weight function so that the forcing term adapts to the velocity component, $\tilde{}$ is a spatial average, and α_B is a relaxation parameter. This forcing was introduced so that the averaged LES velocity field can match the RANS velocity field computed in advance. Although the purpose of the procedure is different from ours, the operator $\tilde{}$ seems to play a similar role to the additional filtering as a filtering procedure.

The additional filtering discussed in this section is valid for channel flow, in which the turbulent field is homogeneous in the x and z directions. More general methods need to be developed for practical simulations of complex flows. Here, we discuss a possible method to generalize the additional filtering. First, the finite difference scheme of the filtered equations can be extended as follows. When the distribution of ℓ and ℓ_R is given in advance, that of the blending parameter is obtained from $\alpha = \ell/\ell_R$. As an example, we treat the case of $\alpha = \alpha(x,y)$ where $\partial\alpha/\partial x < 0$ and $\partial\alpha/\partial y < 0$. The filtered continuity equation can then be written as

$$\frac{\partial\bar{u}_k}{\partial x_k} - \frac{\partial\alpha}{\partial x_k}\frac{\partial\bar{u}_k}{\partial\alpha} = \frac{\bar{u}^{++x}_{i+1/2,j} - \bar{u}_{i-1/2,j}}{\Delta x} + \frac{\bar{v}^{++y}_{ij+1/2} - \bar{v}_{ij-1/2}}{\Delta y} + \left(\frac{\partial\bar{w}}{\partial z}\right)_{ij}, \tag{33}$$

where

$$\bar{u}^{++x}_{i+1/2,j} = \left[G\left(\sqrt{\alpha^2_{i-1/2,j}-\alpha^2_{i+1/2,j}}\right) * \bar{u}\right]_{i+1/2,j}, \tag{34}$$

$$\bar{v}^{++y}_{ij+1/2} = \left[G\left(\sqrt{\alpha^2_{ij-1/2}-\alpha^2_{ij+1/2}}\right) * \bar{v}\right]_{ij+1/2}. \tag{35}$$

The effect of $\partial\alpha/\partial x_k$ can be taken into account by the additional filtering at points $(i,j+1/2)$ and $(i+1/2,j)$ as shown in Eq. (34) and (35), respectively.

Next, we need to define the filtering G for general cases. One possible way is to extend the plane average given by Eqs. (6)–(9) to general cases in a straightforward manner as follows:

$$\bar{u}_k(\mathbf{x}) = \int_{\mathbf{x}-\mathbf{x}' \perp \nabla\alpha(\mathbf{x})} dS G(\mathbf{x}-\mathbf{x}', \alpha) u_k(\mathbf{x}'), \tag{36}$$

$$G(\mathbf{x}, \alpha) = \frac{6}{\pi \ell^2} \exp\left(-6\frac{|\mathbf{x}|^2}{\ell^2}\right), \quad \ell = \alpha \ell_R. \tag{37}$$

In Eq. (36), the integral is taken over a plane perpendicular to the direction of $\nabla\alpha$. The turbulent field is not always homogeneous over this plane, but the plane is located along the RANS/LES interface locally. We should note that the hybrid filter defined as Eqs. (6)–(9) was introduced to just bridge RANS and LES near the interface using the additional filtering (and some defiltering if possible); the definition of the hybrid filter is not directly used in the simulation in the RANS and LES regions. Therefore, we may adopt this plane average as a coarse graining along the interface just to bridge the two models.

Another way to define the filtering G for general cases is to adopt an alternative method corresponding to ensemble average. It is not easy to formulate such a method; the situation is similar to the averaging procedure in the dynamic subgrid-scale model (Meneveau and Katz, 2000). The Lagrangian dynamic model proposed by Meneveau et al. (1996) used averaging over flow pathline by backwards time integration. Such a generalization of the present additional filtering must be interesting. In future work the additional filtering should be extended so that it apply to more complex flows including recirculating flows.

4. Application to channel flow simulation

In order to validate the expression for the filter width derived in the preceding section, we carry out a hybrid RANS/LES simulation of channel flow. The numerical method is the same as that used by Hamba (2006). We solve the filtered Navier–Stokes and continuity equations given by

$$\frac{\partial \bar{u}_k}{\partial t} = -\frac{\partial}{\partial x_m}\bar{u}_m\bar{u}_k - \frac{\partial}{\partial x_m}\tau_{mk} - \frac{\partial \bar{p}}{\partial x_k} + \nu\frac{\partial^2 \bar{u}_k}{\partial x_m \partial x_m} + \delta_{k1}, \tag{38}$$

$$\frac{\partial \bar{u}_k}{\partial x_k} = 0, \tag{39}$$

where

$$\tau_{km} = \overline{u_k u_m} - \bar{u}_k\bar{u}_m, \tag{40}$$

and δ_{km} is the Kronecker delta symbol. Hereafter, all quantities are non-dimensionalized by the wall friction velocity u_τ and the channel half-width $L_y/2$ except for the wall-unit coordinate. The Reynolds number based on u_τ and $L_y/2$ is set to $Re_\tau = 590$ or 5000. The choice of RANS and LES models is an important issue in developing hybrid methods. However, in this work, we do not try to assess and improve RANS and LES models. We adopt simple models and concentrate on the treatment of the log-layer mismatch, which seems to appear irrespective of turbulence model. The Smagorinsky model is used for LES and the corresponding mixing-length model is adopted for RANS. These models are desirable because they explicitly treat the length scale that can be directly related to the blending parameter α. The modeled stress τ_{km} is expressed as

$$\tau_{km} - \frac{1}{3}\tau_{nn}\delta_{km} = -2\nu_T\bar{S}_{km}, \quad \nu_T = (C_S\ell)^2\sqrt{2\bar{S}^2}, \tag{41}$$

where $\bar{S}_{km} = (\partial\bar{u}_k/\partial x_m + \partial\bar{u}_m/\partial x_k)/2$, $\bar{S}^2 = \bar{S}_{km}\bar{S}_{km}$, ν_T is the eddy viscosity, and $C_S(=0.1)$ is the Smagorinsky constant. The length scale ℓ is determined as

$$\ell = \begin{cases} \ell_R & \text{for } 0 < y^+ \leqslant y_A^+ \\ \Delta(y_B^+) + (\ell_R(y_A^+) - \Delta(y_B^+))(y_B^+ - y^+)/(y_B^+ - y_A^+) & \text{for } y_A^+ < y^+ < y_B^+ \\ \Delta & \text{for } y_B^+ \leqslant y^+ \leqslant Re_\tau \end{cases}, \tag{42}$$

where ℓ_R is the RANS length scale and Δ is the representative grid spacing defined as

$$\Delta = [(\Delta x^2 + \Delta y^2 + \Delta z^2)/3]^{1/2}. \tag{43}$$

The RANS region is located at $0 < y^+ \leqslant y_A^+$ and the LES region is at $y_B^+ \leqslant y^+ \leqslant Re_\tau$. We set the buffer region $y_A^+ < y^+ < y_B^+$ to avoid a very rapid change in the length scale ℓ. The value of ℓ_R is determined in advance using the DNS data of Moser et al. (1999) for $Re_\tau = 590$ and the one-dimensional k–ε model simulation for $Re_\tau = 5000$ (see Hamba (2006) for detail).

As shown in Eqs. (12) and (13), the filtered velocity equations originally involve extra terms due to the non-commutivity between the hybrid filter and the spatial derivative. In order to incorporate the effect of the extra terms into the hybrid simulation, we apply the additional filtering to the continuity equation and to the convection terms in the Navier–Stokes equation. The additional filtering is also used when evaluating the modeled and viscous stresses such as $-(\nu_T + \nu)\bar{S}_{km}$, but it is not applied to the pressure-gradient term or to the terms of the gradient of modeled and viscous stresses in the Navier–Stokes equation in order to avoid numerical instability. The reason for the instability is explained in Appendix.

In the previous simulation (Hamba, 2006), the filter width and its location for the additional filtering were determined empirically; they were tuned so that good velocity profiles can be obtained. In the present simulation they are determined on the basis of the relation (29). In order to obtain better velocity profiles, we modify Eq. (29) to

$$\widehat{\Delta}_{j+1/2} = C_H\sqrt{\alpha_{j-1/2}^2 - \alpha_{j+1/2}^2}\,\ell_{Rj+1/2}, \tag{44}$$

where C_H is a non-dimensional constant. If the approximation made in the preceding section is good and Eq. (29) is accurate, C_H is equal to unity. In the case of $C_H = 0$ no additional filtering is applied.

Using the above model equations with and without the additional filtering, we carry out a hybrid simulation of channel flow. The size of the computational domain is $L_x \times L_y \times L_z = 2\pi \times 2 \times \pi$. The number of grid points is mainly $N_x \times N_y \times N_z = 64 \times 64 \times 64$ for $Re_\tau = 590$ and $N_x \times N_y \times N_z = 128 \times 132 \times 64$ for $Re_\tau = 5000$. The grid number for each run is described in Table 1. The periodic boundary conditions are used in the x and z directions whereas the no-slip conditions are imposed at the wall. The governing equations are discretized using the second-order finite-difference scheme on a staggered mesh. The time integration is made using the Crank–Nicolson method for the wall-normal diffusion terms and the Adams–Bashforth method for the other terms. The computation was run for a sufficient length of time to be statistically independent of the initial conditions; then statistics such as the mean velocity were accumulated over a time period of 15 or 20 normalized by $(L_y/2)/u_\tau$. Table 1 shows parameters for 11 runs: Cases 1–3 for $Re_\tau = 590$ and Cases 4–11 for $Re_\tau = 5000$. The loca-

Table 1
Parameters for 11 runs of channel flow simulation.

Case	Re_τ	y_A^+	y_B^+	C_H	N_x	N_y	N_z	Δx^+	Δz^+
1	590	151	224	0	64	64	64	58	29
2	590	151	224	1	64	64	64	58	29
3	590	151	224	2	64	64	64	58	29
4	5000	232	346	0	128	132	64	245	245
5	5000	232	346	1	128	132	64	245	245
6	5000	48	55	0	128	132	64	245	245
7	5000	48	55	1	128	132	64	245	245
8	5000	232	346	0	64	132	64	491	245
9	5000	232	346	1	64	132	64	491	245
10	5000	232	346	0	128	132	32	245	491
11	5000	232	346	1	128	132	32	245	491

tion of the RANS/LES interface in Cases 6 and 7 is different from that in Cases 4 and 5. No additional filtering is applied when $C_H = 0$ whereas the additional filtering given by Eq. (44) is applied when $C_H = 1$ and 2. Compared to Cases 4 and 5, the grid number N_x is halved and the grid spacing Δx^+ is doubled in Cases 8 and 9 while N_z is halved and Δz^+ is doubled in Cases 10 and 11.

First, we show results of Cases 1–3 for $Re_\tau = 590$. Fig. 2a shows the profiles of the length scales ℓ, ℓ_R, and Δ as functions of y^+ for Cases 1–3. The length scales are normalized by the channel half width $L_y/2$. The RANS length scale ℓ_R obtained from the DNS data increases to a large value as y^+ increases. On the other hand, the LES length scale Δ, or the representative grid spacing given by Eq. (43) is small and nearly constant. From the two length scales, ℓ is determined using Eq. (42); it decreases rapidly at $y_A^+ < y^+ < y_B^+$. The length scale ℓ is closely related to the eddy viscosity because the eddy viscosity is given by Eq. (41). Fig. 2b shows the profile of the mean eddy viscosity $\langle \nu_T \rangle$ normalized by ν as a function of y^+ for Case 2. Here, $\langle \cdot \rangle$ denotes averaging over the x–z plane and in time. The profiles of $\langle \nu_T \rangle$ for Cases 1 and 3 (not shown here) are nearly the same as that for Case 2. The eddy viscosity is large in the RANS region and small in the LES region in Fig. 2b. This difference in the eddy viscosity is natural because in general, most of the turbulent fluctuations are modeled in RANS whereas they are resolved in LES.

The blending parameter is determined as $\alpha = \ell/\ell_R$ because of Eq. (9). Fig. 3 shows the profiles of α and $\hat{\Delta}$ as functions of y^+ for Case 2. The blending parameter α is equal to unity in the RANS region at $0 < y^+ \leqslant y_A^+$ whereas it has a small value in the LES region at $y_B^+ \leqslant y^+ \leqslant 590$. Like the length scale ℓ, the parameter α also decreases rapidly at $y_A^+ < y^+ < y_B^+$. As a result, the filter width $\hat{\Delta}$ given by Eq. (44) has a large value at $151 \leqslant y^+ \leqslant 238$. Although $\hat{\Delta}$ shows a non-zero value even in the LES region, the additional filtering is applied only at $151 \leqslant y^+ \leqslant 238$ to save computing time.

Fig. 4a shows the profiles of the mean velocity $\langle \bar{u} \rangle$ as a function of y^+ for Cases 1–3. The DNS result of Moser et al. (1999) is also plotted. The mean velocity is normalized by u_τ for each run. Since the value of the external pressure gradient is set to unity in Eq. (39) and statistically steady state is achieved, the value of u_τ is nearly equal to unity in each run. In Case 1 the additional filtering is not applied; the mean velocity clearly shows a steep gradient at $y^+ = y_B^+$ and is overestimated in the LES region as was already reported in several hybrid simulations (Hamba, 2003, 2006; Nikitin et al., 2000; Piomelli et al., 2003). In Case 2 in which the additional filtering is applied with $C_H = 1$, the velocity gradient at $y^+ = y_B^+$ is reduced, but the velocity in the LES region is still overestimated slightly. In Case 3 in which $\hat{\Delta}$ is doubled, a good velocity profile is obtained. This result shows that the additional filtering with the filter width given by Eq. (44) is effective in reducing the log-layer mismatch.

As was discussed in Section 2, it is considered that insufficient resolved velocity fluctuations near the RANS/LES interface is responsible for the log-layer mismatch (Hamba, 2003, 2006; Piomelli et al., 2003). To confirm the explanation, we examine the bal-

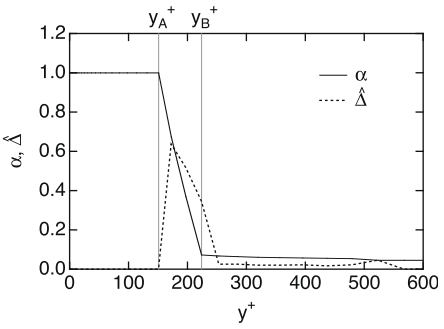

Fig. 3. Profiles of the blending parameter α and the filter width $\hat{\Delta}$ as functions of y^+ for Case 2.

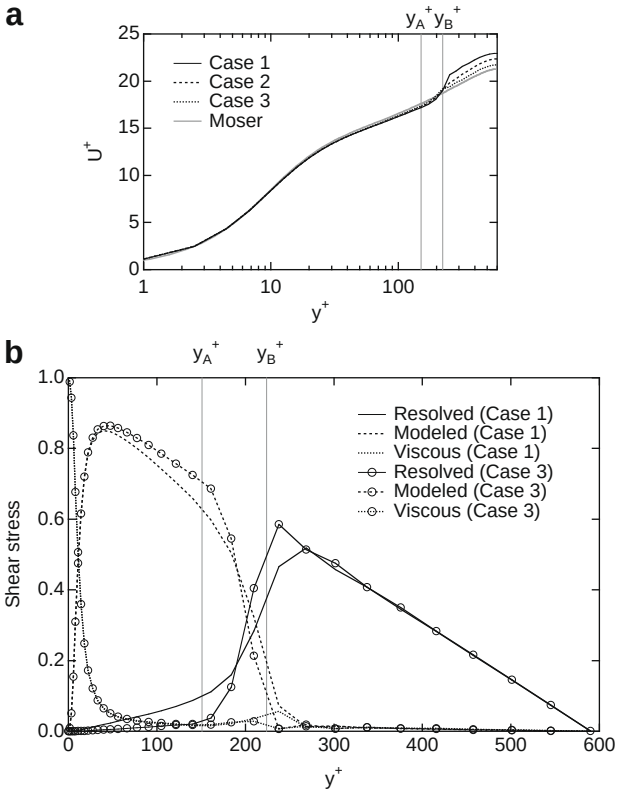

Fig. 4. Profiles of the mean velocity and the shear stresses as functions of y^+: (a) mean velocity $\langle \bar{u} \rangle$ for Cases 1–3 and the DNS result of Moser et al. (1999) and (b) the resolved, modeled, and viscous shear stresses for Cases 1 and 3.

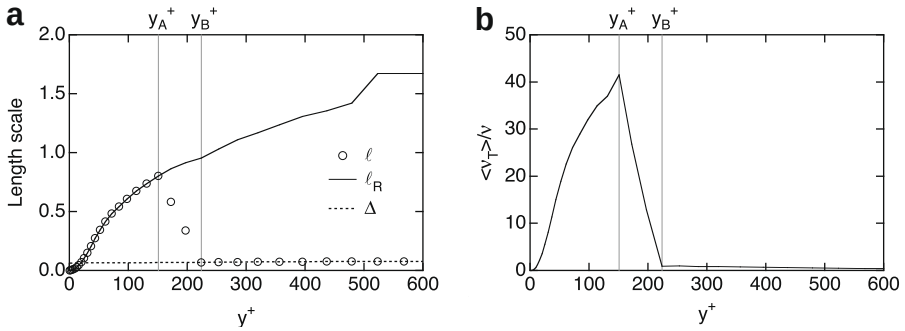

Fig. 2. Profiles of the length scales and the mean eddy viscosity as functions of y^+: (a) ℓ, ℓ_R, and Δ for Cases 1–3 and (b) $\langle \nu_T \rangle / \nu$ for Case 2.

ance of the terms in the mean velocity equation. In a statistically steady state the following relation for the shear stresses holds:

$$1 - y = -\langle \bar{u}'' \bar{v}'' \rangle - \langle \tau_{12} \rangle + \nu \frac{\partial \langle \bar{u} \rangle}{\partial y}, \tag{45}$$

where the three terms on the right-hand side represent the resolved stress, the modeled stress, and the viscous stress, respectively. Fig. 4b shows the three terms for Cases 1 and 3. In both cases the resolved stress shows a small value in the RANS region and a large value in the LES region. However, the increase in the resolved stress across the RANS/LES interface in Case 1 is not much enough compared to that in Case 3. At $y^+ = 238$ in the LES region, the resolved stress in Case 1 is underpredicted although the resolved stress needs to be nearly equal to $1 - y$ in a statistically steady channel flow. The underprediction of the resolved stress leads to the overprediction of the modeled and viscous stresses and is responsible for the steep velocity gradient at $y^+ = y_B^+$. On the other hand, in Case 3 the resolved stress is large enough at $y^+ = 238$ and the velocity gradient has an appropriate value. Therefore, owing to the additional filtering the resolved stress at the bottom of the LES region is restored, eliminating the log-layer mismatch.

Fig. 5 shows the profiles of the streamwise and wall-normal turbulent intensities for Cases 1 and 3. The intensities in the RANS region are fairly small compared with the DNS result. This is natural because most of the velocity fluctuations in the RANS region are represented by the modeled turbulent kinetic energy. As a result, a peak in the profile of the intensities is present after the y_B^+ position. Owing to the additional filtering, the difference in the intensity between the RANS and LES regions becomes greater in Case 3 than in Case 1; this tendency is favorable for the hybrid simulation. It is shown that the underprediction of the resolved shear stress at $y^+ = 238$ is due mainly to the underprediction of the wall-normal intensity. In the core region of channel, the intensities in Case 3 are slightly less than those in Case 1 and the DNS result. It remains as future work to improve the profiles of turbulent intensities in the whole region.

Next, we show results of Cases 4–7 for $Re_\tau = 5000$. Fig. 6 shows the profiles of the mean velocity as a function of y^+ for Cases 4–7. In Cases 4 and 5, the RANS/LES interface is set to $y_A^+ = 232$ and $y_B^+ = 346$. In Case 4 the additional filtering is not applied; the mean velocity shows a steep gradient at $y^+ = y_B^+$ like that in Case 1. Not only the log layer in the LES region is shifted but also the velocity in the RANS region at $y^+ \simeq y_A^+$ is underpredicted. This underprediction is a problem specific to the mixing length model adopted in this work; the reason for the underprediction in Case 4 can be explained as follows. The RANS length scale ℓ_R in the mixing-length model is determined in advance using the one-dimensional solution of the k–ε model in which the resolved velocity field has no three-dimensional fluctuation. However, in the hybrid simulation, the resolved velocity fluctuations are not necessarily very small in the RANS region, leading to inaccurate values of the eddy viscosity and the mean velocity.

On the other hand, in Case 5 the additional filtering is applied and the log-layer mismatch is nearly removed. A good profile is obtained even for $C_H = 1$ because the log-layer mismatch in Case 4 is not as large as that in Case 1. Since the resolved velocity fluctuations are restored in Case 5 (not shown here), the velocity gradient at $y^+ = y_B^+$ has an appropriate value. The velocity profile in the RANS region is also improved because the resolved velocity fluctuations decrease due to the additional filtering. We should note that the steep gradient seen at $y^+ > 1000$ is physical in the wake region of high-Reynolds-number channel flows (Hamba, 2006; Keating and Piomelli, 2006). We set $N_x = 128$ for $Re_\tau = 5000$ because at lower resolution no wake is predicted due to the low-order finite-difference scheme used (Hamba, 2006; Keating and Piomelli, 2006; Cabot et al., 1999).

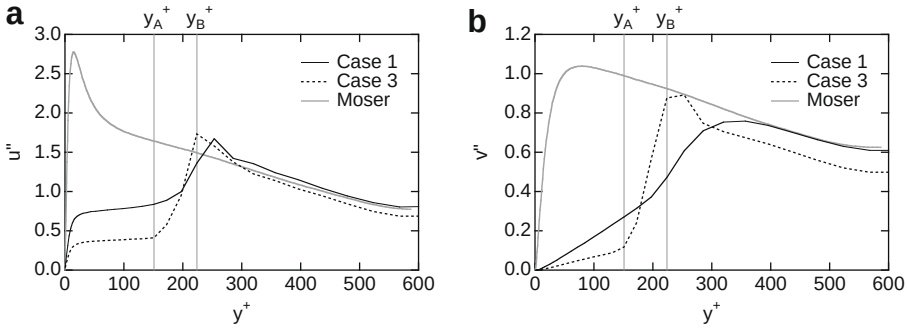

Fig. 5. Profiles of turbulent intensities for Cases 1 and 3 and the DNS result of Moser et al. (1999): (a) streamwise component $\sqrt{\langle \bar{u}''^2 \rangle}$ and (b) wall-normal component $\sqrt{\langle \bar{v}''^2 \rangle}$.

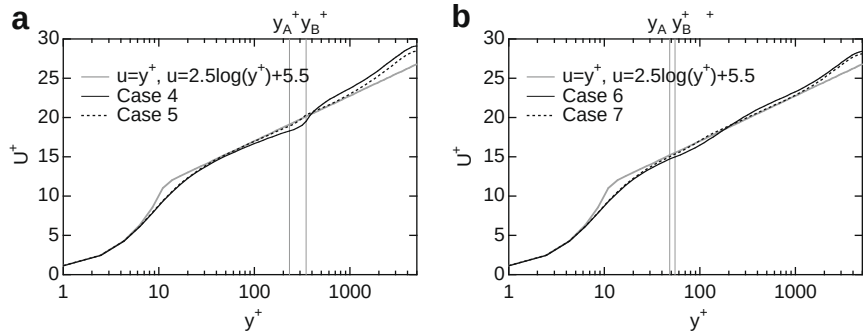

Fig. 6. Profiles of the mean velocity $\langle \bar{u} \rangle$ as functions of y^+: (a) Cases 4 and 5 and (b) Cases 6 and 7.

In order to assess the effect of the interface location, the interface in Cases 6 and 7 is set to $y_A^+ = 48$ and $y_B^+ = 55$ closer to the wall. The log-layer mismatch is seen in Case 6 whereas it is removed and a good profile is obtained in Case 7 in Fig. 6b. Compared to the result of Case 4, the position of the unphysical buffer layer relative to the RANS/LES interface in Case 6 is somewhat different. The steep velocity gradient is seen in the region fairly apart from the interface in Case 6 in contrast to Cases 1 and 4.

To explain the reason for the difference, we examine the length scales. Fig. 7a shows the profiles of the length scales ℓ, ℓ_R, and Δ as functions of y^+ for Cases 5 and 7. The RANS (LES) length scale is common in the two cases. Since the RANS/LES interface is away from the wall in Case 5, the length scale ℓ decreases rapidly at $y_A^+ < y^+ < y_B^+$; its value at $y_A^+ = 232$ is much greater that that at $y_B^+ = 346$. On the other hand, the RANS/LES interface in Case 7 is set to the location where ℓ_R is nearly equal to Δ. The length scale ℓ is connected at the RANS/LES interface without overshoot, as is the case of previous DES calculations (Nikitin et al., 2000; Piomelli et al., 2003).

Fig. 7b shows the profiles of the mean eddy viscosity $\langle \nu_T \rangle$ as a function of y^+ for Cases 5 and 7. The profiles of $\langle \nu_T \rangle$ in Fig. 7b are similar to those of ℓ in Fig. 7a; the eddy viscosity in Case 5 decreases rapidly at $y_A^+ < y^+ < y_B^+$ whereas that in Case 7 is connected without overshoot. The profiles of the eddy viscosity in Cases 4 and 6 (not shown here) are nearly the same as those in Cases 5 and 7, respectively. The log-layer mismatch is seen not only in Case 4 in which the eddy viscosity decreases rapidly at the RANS/LES interface, but also in Case 6 in which the eddy viscosity is connected without overshoot. The unphysical buffer layer in Case 4 is seen at $y^+ = y_B^+$ where the eddy viscosity decreases rapidly. On the other hand, the unphysical buffer layer in Case 6 is not seen at the interface where the gradient of the eddy viscosity changes suddenly, but it is seen at $y^+ \simeq 200$ in the LES region apart from the interface. Therefore, the sudden change in the eddy viscosity or its gradient at the RANS/LES interface is not necessarily the main reason for the log-layer mismatch.

Fig. 8 shows the profiles of the blending parameter α and the filter width $\widehat{\Delta}$ as functions of y^+ for Cases 5 and 7. In Case 5 the blending parameter decreases rapidly at the interface at $y_A^+ < y^+ < y_B^+$ like that in Case 1 shown in Fig. 3. On the other hand, in Case 7 the blending parameter changes very little at $y_A^+ < y^+ < y_B^+$, but it decreases gradually as y^+ increases in the LES region apart from the interface. The decrease in α in the LES region in Case 7 is due to the increase in ℓ_R; that is, since $\ell(= \Delta)$ is nearly constant and ℓ_R increases, α decreases gradually in the LES region. The location of the decrease in α in Fig. 7 corresponds to the location of the unphysical buffer layer in Fig. 5. This result is consistent with the discussion in Section 3 that the extra terms involving the gradient of α cannot be neglected. It is suggested that the neglect of the extra terms is responsible for the log-layer mismatch. In this

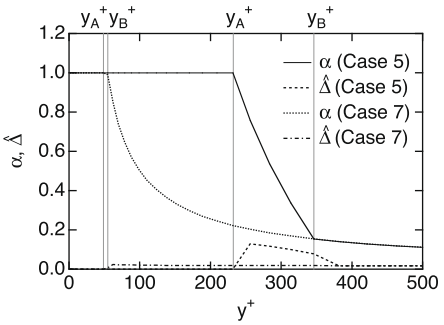

Fig. 8. Profiles of the blending parameter α and the filter width $\widehat{\Delta}$ as functions of y^+ for Cases 5 and 7.

work, to incorporate the effect of the extra terms, the additional filtering is applied with the filter width $\widehat{\Delta}$. In Case 5, the filter width $\widehat{\Delta}$ has a large value at the RANS/LES interface as shown in Fig. 8. On the other hand, in Case 7 $\widehat{\Delta}$ shows a small but non-zero value in the LES region because the gradient of α has a finite value. Since it takes much computing time to apply the additional filtering in the whole LES region, we applied it only at $51 < y^+ < 145$ in Case 7. Nevertheless, a good velocity profile is obtained in Case 7 as well as in Case 5 as shown in Fig. 6. This result shows that the expression for $\widehat{\Delta}$ given by Eq. (44) is appropriate in both cases where the eddy viscosity is connected at the interface in a different manner.

Finally, we examine the sensitivity of the results with respect to the size of the grid cells. As shown in Table 1, the grid spacing in the streamwise direction is doubled in Cases 8 and 9 and that in the spanwise direction is doubled in Cases 10 and 11. The size of the computational domain is unchanged. Fig. 9a shows the profiles of the mean velocity as a function of y^+ for Cases 8–11. In Cases 9 and 11 where C_H is set to unity the velocity mismatch is reduced; the additional filtering is effective in these coarse meshes. However, the velocity profiles in the core region in Cases 8 and 9 are different from those in Cases 4 and 5 plotted in Fig. 6a. The steep gradient at $y^+ > 1000$ is not seen in Cases 8 and 9. Due to the coarse grid in the streamwise direction, no wake is predicted (Hamba, 2006; Keating and Piomelli, 2006; Cabot et al., 1999). On the other hand, in Cases 10 and 11, the mean velocity is well predicted whereas the turbulent intensities in the core region is poorly predicted. Fig. 9b shows the profiles of the wall-normal intensity $\sqrt{\langle \tilde{v}''^2 \rangle}$ as a function of y^+ in Cases 5, 9, and 11. In Cases 5 and 9 where $\Delta z^+ = 245$, the intensity decreases monotonically as y^+ increases in the core region. However, in Case 11 where $\Delta z^+ = 491$, the intensity begins to increase at $y^+ = 3800$ and reaches a fairly large value at the channel center. This artificial increase is due to the coarse grid in the spanwise direction. Therefore, the results in Cases 8–11 are inaccurate and the grid cells

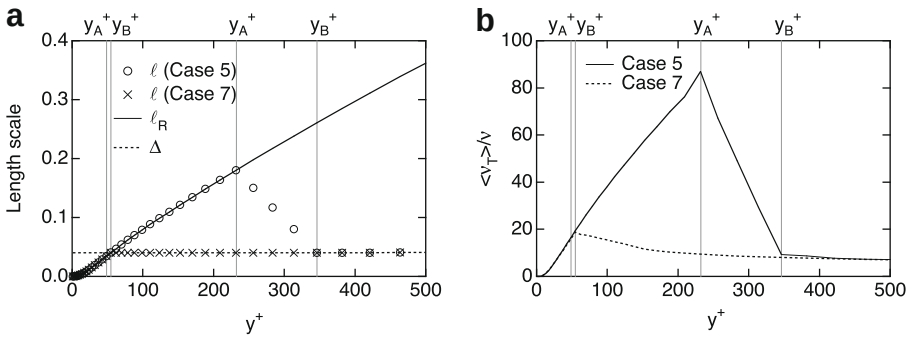

Fig. 7. Profiles of the length scales and the mean eddy viscosity as functions of y^+ for Cases 5 and 7: (a) ℓ, ℓ_R, and Δ and (b) $\langle \nu_T \rangle / \nu$.

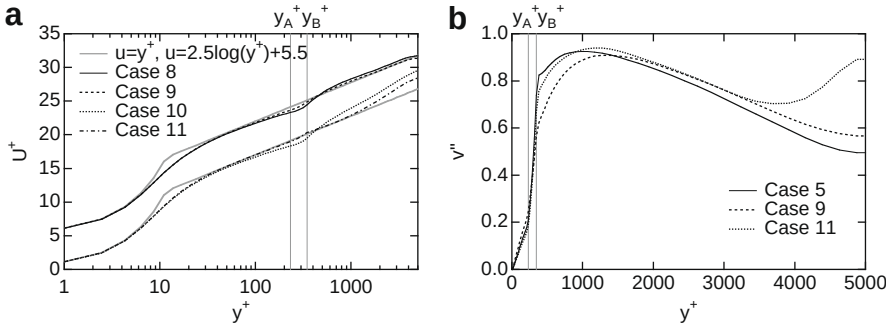

Fig. 9. Profiles of the mean velocity and the wall-normal intensity as functions of y^+: (a) mean velocity $\langle\bar{u}\rangle$ for Cases 8–11 and (b) wall-normal intensity $\sqrt{\langle\bar{v}''^2\rangle}$ for Cases 5, 9, and 11.

with $\Delta x^+ = \Delta z^+ = 245$ are necessary for accurate simulation of this channel flow.

The case of $Re_\tau = 5000$ was investigated as an example of high Reynolds numbers. In the case of low Reynolds number $Re_\tau < 590$, the mean velocity profile with and without additional filtering is basically the same as that for $Re_\tau = 590$. However, when Re_τ is so low that the RANS/LES interface is located within the physical buffer layer between the logarithmic layer and the viscous sub-layer, the steep gradient due to mismatch is somewhat unclear because it is overlapped by the gradient of the buffer layer as shown in Case A1 ($Re_\tau = 180$) plotted in Fig. 2 of Nikitin et al. (2000).

5. Conclusions

It is known that log-layer mismatch appears in hybrid RANS/LES simulations of channel flow. Although several methods have been proposed to eliminate the log-layer mismatch, there is no obvious physical justification for the methods. To justify the method of additional filtering at the RANS/LES interface proposed by Hamba (2003), we examined the commutation error in the filtered velocity equations. A two-dimensional filtering with the filter width ranging from the grid size to the RANS length scale is introduced as a hybrid filter. The filtered equations involve extra terms due to the non-commutivity between the filtering and the spatial derivative. It was shown that the additional filtering can be considered as a finite difference approximation to the extra terms. We obtained an expression determining the filter width and its location for the additional filtering. To validate this expression, a hybrid simulation of channel flow was carried out with the Smagorinsky and mixing-length models. The unphysical buffer layer is located in the region where the blending parameter decreases. This result suggests that the neglect of the extra terms due to the non-commutivity is responsible for the log-layer mismatch. It was shown that the additional filtering with the filter width derived is effective in eliminating the log-layer mismatch and this improvement is because sufficient resolved velocity fluctuations are generated at the bottom of the LES region.

In the present work, a two-dimensional filtering in the wall-parallel directions is used as the additional filtering to improve the hybrid simulation of channel flow. As future work, the method of additional filtering needs to be extended to general turbulent flows. Moreover, instead of the mixing length model, more general models such as the k–ε model should be adopted for RANS for practical hybrid simulations.

Acknowledgement

This work was partially supported by the Grant-in-Aid for Scientific Research of Japan Society for the Promotion of Science (16560315).

Appendix

The extra terms due to the non-commutivity appear not only for the convection terms but also for the pressure-gradient and diffusion terms in the Navier–Stokes equation given by Eq. (13). From a theoretical point of view, the additional filtering should be applied to all the extra terms. However, in this work, the additional filtering is not applied when evaluating the gradient of the pressure and those of the modeled and viscous stresses in Eq. (13) to avoid numerical instability. The reason for the numerical instability can roughly be explained as follows.

If the additional filtering is applied to the pressure-gradient term, it can be written as

$$\overline{\frac{\partial p}{\partial y}}_{i,j+1/2} = \left(\frac{\partial \bar{p}}{\partial y} - \frac{\partial \alpha}{\partial y}\frac{\partial \bar{p}}{\partial \alpha}\right)_{i,j+1/2} = \frac{\hat{\bar{p}}_{i,j+1} - \bar{p}_{i,j}}{\Delta y}. \tag{A1}$$

In the Poisson equation for the pressure, the second derivative of the pressure in the y direction can then be expressed as

$$\overline{\frac{\partial^2 p}{\partial y^2}}_{i,j} = \frac{1}{\Delta y}\left(\frac{\hat{\bar{p}}_{i,j+1} - \hat{\bar{p}}_{i,j}}{\Delta y} - \frac{\hat{\bar{p}}_{i,j} - \bar{p}_{i,j-1}}{\Delta y}\right). \tag{A2}$$

The Poisson equation is solved using the Fourier transform in the x and z directions. Hereafter, we omit the dependence on the z coordinate for simplicity. The Fourier component $\tilde{f}$ of a physical quantity f can be written as

$$f_{i,j} = \sum_{i'=-N/2}^{N/2-1} \tilde{f}_{i',j} \exp(2\pi I i i'/N_x), \tag{A3}$$

where $I = \sqrt{-1}$. The Fourier components of the filtered pressures appearing in Eq. (A2) can be written as

$$\hat{\tilde{\bar{p}}}_{i',j} = \hat{g}_{i'}\tilde{\bar{p}}_{i',j}, \quad \hat{\hat{\tilde{\bar{p}}}}_{i',j} = \hat{g}_{i'}^2\tilde{\bar{p}}_{i',j}, \tag{A4}$$

where the filter function $\hat{g}_{i'}$ is given by

$$\hat{g}_{i'} = \exp[-(2\pi i'/N_x)^2/24], \tag{A5}$$

for the Gaussian filter. The left-hand side of the Poisson equation given by

$$\left(\overline{\frac{\partial^2 p}{\partial x^2}} + \overline{\frac{\partial^2 p}{\partial y^2}}\right)_{i,j}, \tag{A6}$$

can be expressed in terms of the Fourier components as

$$\frac{\hat{g}_{i'}^2}{(\Delta y)^2}\tilde{\bar{p}}_{i',j+1} - \left[k_{i'}^2 + \frac{2\hat{g}_{i'}}{(\Delta y)^2}\right]\tilde{\bar{p}}_{i',j} + \frac{1}{(\Delta y)^2}\tilde{\bar{p}}_{i',j-1}, \tag{A7}$$

where

$$k_{i'} = \frac{2}{\Delta x}\sin(\pi i'/N_x). \tag{A8}$$

In order to solve the tridiagonal system of equations keeping the round-off errors down, the coefficient for $\tilde{\bar{p}}_{i'j}$ needs to be greater than the sum of those for $\tilde{\bar{p}}_{i'j+1}$ and $\tilde{\bar{p}}_{i'j-1}$ as follows (Roache, 1976):

$$k_{i'}^2 + \frac{2\hat{g}_{i'}}{(\Delta y)^2} > \frac{\hat{g}_{i'}^2}{(\Delta y)^2} + \frac{1}{(\Delta y)^2}. \tag{A9}$$

However, this condition does not hold for a large value of $(\hat{g}_{i'}-1)^2/(\Delta y)^2$, which accounts for the instability of the expression (A2).

In this work, the additional filtering is not applied to the pressure-gradient term; it is applied only when taking the divergence of the Navier–Stokes equation to obtain the Poisson equation. The second derivative terms in the Poisson equation can be expressed as

$$\overline{\frac{\partial^2 p}{\partial y^2}}_{ij} = \frac{1}{\Delta y}\left(\frac{\hat{\bar{p}}_{i,j+1}-\hat{\bar{p}}_{ij}}{\Delta y} - \frac{\bar{p}_{ij}-\bar{p}_{i,j-1}}{\Delta y}\right), \tag{A10}$$

which corresponds to the y derivative terms on the left-hand side of Eq. (25). It is expressed in terms of the Fourier components as

$$\frac{\hat{g}_{i'}}{(\Delta y)^2}\tilde{\bar{p}}_{i'j+1} - \left[k_{i'}^2 + \frac{\hat{g}_{i'}+1}{(\Delta y)^2}\right]\tilde{\bar{p}}_{i'j} + \frac{1}{(\Delta y)^2}\tilde{\bar{p}}_{i'j-1}. \tag{A11}$$

In this case, the condition for the coefficients

$$k_{i'}^2 + \frac{\hat{g}_{i'}+1}{(\Delta y)^2} > \frac{\hat{g}_{i'}}{(\Delta y)^2} + \frac{1}{(\Delta y)^2}, \tag{A12}$$

holds for an arbitrary value of $\hat{g}_{i'}$. Therefore, the Poisson equation with Eq. (A10) can be solved.

Next, we explain the stability requirement for the diffusion terms. Here, for simplicity we consider the Euler scheme for time marching and treat only the molecular viscosity which is constant in space. If the additional filtering is applied not only to the evaluation of the viscous stress but also to the gradient of the stress in the Navier–Stokes equation, the diffusion term in the y direction as well as the time derivative term can be written as

$$\frac{\bar{u}_{ij}^{n+1}-\bar{u}_{ij}^{n}}{\Delta t} = \nu\frac{1}{\Delta y}\left(\frac{\hat{\bar{u}}_{i,j+1}^{n}-\hat{\bar{u}}_{ij}^{n}}{\Delta y} - \frac{\hat{\bar{u}}_{ij}^{n}-\hat{\bar{u}}_{i,j-1}^{n}}{\Delta y}\right), \tag{A13}$$

where the superscript n stands for the time step. It is expressed in terms of the Fourier components as

$$\frac{\tilde{\bar{u}}_{i'j}^{n+1}-\tilde{\bar{u}}_{i'j}^{n}}{\Delta t} = \nu\frac{1}{\Delta y}\left(\frac{\hat{g}_{i'}^2\tilde{\bar{u}}_{i'j+1}^{n} - \hat{g}_{i'}\tilde{\bar{u}}_{i'j}^{n}}{\Delta y} - \frac{\hat{g}_{i'}\tilde{\bar{u}}_{i'j}^{n} - \tilde{\bar{u}}_{i'j-1}^{n}}{\Delta y}\right). \tag{A14}$$

Moreover, we apply the von Neumann stability analysis by using the Fourier transform in the y direction (Roache, 1976)

$$\tilde{\bar{u}}_{i'j}^{n} = u^n \exp[Ik_y j\Delta y], \tag{A15}$$

where u^n is the amplitude function at time step n. The diffusion equation (A14) can be written as

$$\frac{u^{n+1}-u^n}{\Delta t} = \frac{\nu}{(\Delta y)^2}[\hat{g}_{i'}^2\exp(Ik_y\Delta y) - 2\hat{g}_{i'} + \exp(-Ik_y\Delta y)]u^n, \tag{A16}$$

The amplification factor $A(=u^{n+1}/u^n)$ can then be given by

$$A = 1 - \frac{\nu\Delta t}{(\Delta y)^2}[2(\hat{g}_{i'}^2+1)\sin^2\theta - (\hat{g}_{i'}-1)^2 - 2I(\hat{g}_{i'}^2-1)\sin\theta\cos\theta], \tag{A17}$$

where $\theta = k_y\Delta y/2$. The magnitude $|A|$ should be less than unity for stability. However, If the value of θ is so small that $\sin\theta$ can be neglected in Eq. (A17), the factor A can be written as

$$A = 1 + \frac{\nu\Delta t}{(\Delta y)^2}(\hat{g}_{i'}-1)^2. \tag{A18}$$

Since this factor is always greater than unity for arbitrary Δt, the stability requirement cannot be satisfied. For the Crank–Nicolson scheme the factor A is given by

$$A = \left[1 + \frac{\nu\Delta t}{2(\Delta y)^2}(\hat{g}_{i'}-1)^2\right] \Big/ \left[1 - \frac{\nu\Delta t}{2(\Delta y)^2}(\hat{g}_{i'}-1)^2\right], \tag{A19}$$

which is also greater than unity. The diffusion Eq. (A13) cannot be solved even using the Crank–Nicolson scheme.

In this work, the additional filtering is not applied when evaluating the gradient of the viscous stress in the Navier–Stokes equation as follows:

$$\frac{\bar{u}_{ij}^{n+1}-\bar{u}_{ij}^{n}}{\Delta t} = \nu\frac{1}{\Delta y}\left(\frac{\hat{\bar{u}}_{i,j+1}^{n}-\bar{u}_{ij}^{n}}{\Delta y} - \frac{\hat{\bar{u}}_{ij}^{n}-\bar{u}_{i,j-1}^{n}}{\Delta y}\right). \tag{A20}$$

This equation can be rewritten as

$$\frac{u^{n+1}-u^n}{\Delta t} = \frac{\nu}{(\Delta y)^2}[\hat{g}_{i'}\exp(Ik_y\Delta y) - (\hat{g}_{i'}+1) + \exp(-Ik_y\Delta y)]u^n. \tag{A21}$$

The amplification factor is then given by

$$A = 1 - \frac{\nu\Delta t}{(\Delta y)^2}[2(\hat{g}_{i'}+1)\sin^2\theta - 2I(\hat{g}_{i'}-1)\sin\theta\cos\theta]. \tag{A22}$$

In this expression, there is no positive term like $(\hat{g}_{i'}-1)^2$. Therefore, if Δt is small enough, the magnitude $|A|$ can be less than unity; the stability requirement can be satisfied.

The instability for the pressure-gradient and diffusion terms seems to be caused by the application of the filtering twice without defiltering because Eqs. (A9) and (A18) both involve $\hat{g}_{i'}^2$. We expect that if some defiltering procedure corresponding to $\hat{g}_{i'}^{-1}$ is applied using Eq. (19) in future work, this difficulty can be overcome and the additional filtering can fully be applied to the pressure-gradient and diffusion terms.

References

Abe, K., 2005. A hybrid LES/RANS approach using an anisotropy-resolving algebraic turbulence model. Int. J. Heat Fluid Flow 26, 204–222.

Batten, P., Goldberg, U., Chakravarthy, S., 2004. Interfacing statistical turbulence closures with large-eddy simulation. AIAA J. 42, 485–492.

Befeno, I., Schiestel, R., 2007. Non-equilibrium mixing of turbulence scales using a continuous hybrid RANS/LES approach: application to the shearless mixing layer. Flow Turbulence Combust. 78, 129–151.

Benarafa, Y., Cioni, O., Ducros, F., Sagaut, P., 2006. RANS/LES coupling for unsteady turbulent flow simulation at high Reynolds number on coarse meshes. Comput. Methods Appl. Mech. Eng. 195, 2939–2960.

Breuer, M., Jaffrézic, B., Arora, K., 2008. Hybrid LES–RANS technique based on a one-equation near-wall model. Theor. Comput. Fluid Dyn. 22, 157–187.

Cabot, W., Jiménez, J., Baggett, J.S., 1999. On wakes and near-wall behavior in coarse large-eddy simulation of channel flow with wall models and second-order finite-difference methods. In: Center for Turbulence Research, Annual Research Briefs. Stanford University, pp. 343–354.

Davidson, L., Dahlström, S., 2005. Hybrid LES-RANS: an approach to make LES applicable at high Reynolds number. Int. J. Comput. Fluid Dyn. 19, 415–427.

Davidson, L., Peng, S.H., 2003. Hybrid LES-RANS modelling: a one-equation SGS model combined with a k–ω model for predicting recirculating flows. Int. J. Numer. Methods Fluids 43, 1003–1018.

Fureby, C., Tabor, G., 1997. Mathematical and physical constraints on large-eddy simulations. Theoret. Comput. Fluid Dyn. 9, 85–102.

Fureby, C., Alin, N., Wikström, N., Menon, S., Svanstedt, N., Persson, L., 1997. Large-eddy simulation of high-Reynolds-number wall-bounded flows. AIAA J. 42, 457–468.

Georgiadis, N.J., Alexander, J.I.D., Reshotko, E., 2003. Hybrid Reynolds-averaged Navier–Stokes/large-eddy simulations of supersonic turbulent mixing. AIAA J. 41, 218–229.

Germano, M., 2004. Properties of the hybrid RANS/LES filter. Theoret. Comput. Fluid Dyn. 17, 225–231.

Hamba, F., 2001. An attempt to combine large eddy simulation with the k–ε model in a channel-flow calculation. Theoret. Comput. Fluid Dyn. 14, 323–336.

Hamba, F., 2003. A hybrid RANS/LES simulation of turbulent channel flow. Theoret. Comput. Fluid Dyn. 16, 387–403.

Hamba, F., 2005. Nonlocal analysis of the Reynolds stress in turbulent shear flow. Phys. Fluids 17, 115102.
Hamba, F., 2006. A hybrid RANS/LES simulation of high-Reynolds-number channel flow using additional filtering at the interface. Theoret. Comput. Fluid Dyn. 20, 89–101.
Hanjalic, K., 2005. Will RANS survive LES? A view of perspectives. J. Fluid Eng. 127, 831–839.
Kawai, S., Fujii, K., 2005. Computational study of a supersonic base flow using hybrid turbulence methodology. AIAA J. 43, 1265–1275.
Keating, A., Piomelli, U., 2006. A dynamic stochastic forcing method as a wall-layer model for large-eddy simulation. J. Turbulence 7 (12), 1–24.
Kenjereš, S., Hanjalić, K., 2006. LES, T-RANS and hybrid simulations of thermal convection at high Ra numbers. Int. J. Heat Fluid Flow 27, 800–810.
Labourasse, E., Sagaut, P., 2002. Reconstruction of turbulent fluctuations using a hybrid RANS/LES approach. J. Comput. Phys. 182, 301–336.
Larsson, J., Lien, F.S., Yee, E., 2007. The artificial buffer layer and the effects of forcing in hybrid LES/RANS. Int. J. Heat Fluid Flow 28, 1443–1459.
Meneveau, C., Katz, J., 2000. Scale-invariance and turbulence models for large-eddy simulation. Annu. Rev. Fluid Mech. 32, 1–32.
Meneveau, C., Lund, T.S., Cabot, W.H., 1996. A Lagrangian dynamic subgrid-scale model of turbulence. J. Fluid Mech. 319, 353–385.
Moser, R.D., Kim, J., Mansour, N.N., 1999. Direct numerical simulation of turbulent channel flow up to $Re_\tau = 590$. Phys. Fluids 11, 943–945.
Nikitin, N.V., Nicoud, F., Wasistho, B., Squires, K.D., Spalart, P.R., 2000. An approach to wall modeling in large-eddy simulations. Phys. Fluids 12, 1629–1632.
Piomelli, U., Balaras, E., Pasinato, H., Squires, K.D., Spalart, P.R., 2003. The inner–outer layer interface in large-eddy simulations with wall-layer models. Int. J. Heat Fluid Flow 24, 538–550.
Quéméré, P., Sagaut, P., 2002. Zonal multi-domain RANS/LES simulations of turbulent flows. Int. J. Numer. Methods Fluids 40, 903–925.
Quéméré, P., Sagaut, P., Couailler, V., 2001. A new multi-domain/multi-resolution method for large-eddy simulation. Int. J. Numer. Methods Fluids 36, 391–416.
Radhakrishnan, S., Piomelli, U., Keating, A., Lopes, A.S., 2006. Reynolds-averaged and large-eddy simulations of turbulent non-equilibrium flows. J. Turbulence 7 (63), 1–30.
Roache, P.J., 1976. Computational Fluid Dynamics. Hermosa Publishers, Albuquerque.
Sagaut, P., Deck, S., Terracol, M., 2006. Multiscale and Multiresolution Approaches in Turbulence. Imperial College Press, London.
Schiestel, R., Dejoan, A., 2005. Towards a new partially integrated transport model for coarse grid and unsteady turbulent flow simulations. Theoret. Comput. Fluid Dyn. 18, 443–468.
Spalart, P.R., Allmaras, S.R., 1994. A one-equation turbulence model for aerodynamic flows. La Recherche Aerospatiale 1, 5–21.
Spalart, P.R., Jou, W.H., Strelets, M., Allmaras, S.R., 1997. Comments on the feasibility of LES for wings, and on a hybrid RANS/LES approach. In: Proc. First AFOSR International Conference on DNS/LES, pp. 137–147.
Spalart, P.R., Deck, S., Shur, M.L., Squires, K.D., Strelets, M.Kh., Travin, A., 2006. A new version of detached-eddy simulation, resistant to ambiguous grid densities. Theoret. Comput. Fluid Dyn. 20, 181–195.
Temmerman, L., Hadžiabdić, M., Leschziner, M.A., Hanjalić, K., 2005. A hybrid two-layer URANS-LES approach for large eddy simulation at high Reynolds numbers. Int. J. Heat Fluid Flow 26, 173–190.
Tucker, P.G., Davidson, L., 2004. Zonal k–l based large eddy simulations. Comput. Fluids 33, 267–287.